



# Facile synthesis of Cu(II) impregnated biochar with enhanced adsorption activity for the removal of doxycycline hydrochloride from water



Su Liu <sup>a,b</sup>, Wei-hua Xu <sup>a,b,\*</sup>, Yun-guo Liu <sup>a,b,\*</sup>, Xiao-fei Tan <sup>a,b</sup>, Guang-ming Zeng <sup>a,b</sup>, Xin Li <sup>a,b</sup>, Jie Liang <sup>a,b</sup>, Zan Zhou <sup>a,b</sup>, Zhi-li Yan <sup>a,b</sup>, Xiao-xi Cai <sup>a,b,c</sup>

<sup>a</sup> College of Environmental Science and Engineering, Hunan University, Changsha 410082, PR China

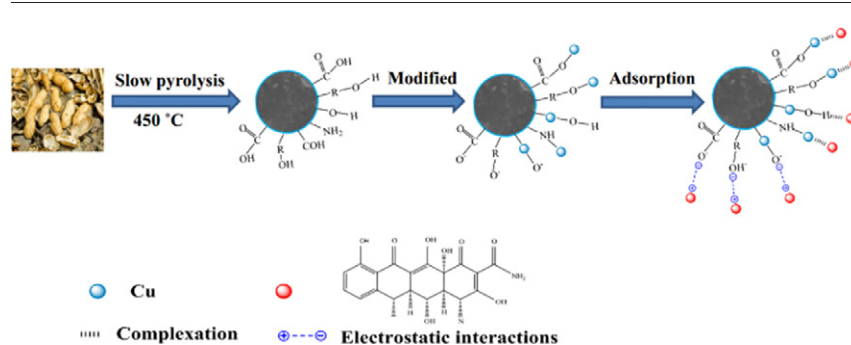
<sup>b</sup> Key Laboratory of Environmental Biology and Pollution Control, Hunan University, Ministry of Education, Changsha 410082, PR China

<sup>c</sup> College of Art and Design, Hunan First Normal University, Changsha 410205, PR China

## HIGHLIGHTS

- Biochar derived from agricultural wastes were low-cost.
- Cu(II) modified biochar exhibited excellent sorption efficiency compared with pristine biochar.
- Efficiency of DOX removal was greatly pH dependent.
- Cu(II) strongly enhanced the sorption of DOX species through complexation.

## GRAPHICAL ABSTRACT



## ARTICLE INFO

### Article history:

Received 6 January 2017

Received in revised form 2 March 2017

Accepted 9 March 2017

Available online 17 March 2017

Editor: D. Barcelo

### Keywords:

Biochar

DOX

Adsorption

Copper modification

Water treatment

## ABSTRACT

In this study, the effect factors and mechanisms of doxycycline hydrochloride (DOX) adsorption on copper nitrate modified biochar (Cu-BC) was investigated. Cu-BC adsorbent was synthesized through calcination of peanut shells biomass at 450 °C and then impregnation with copper nitrate. The Cu-BC has exhibited excellent sorption efficiency about 93.22% of doxycycline hydrochloride from aqueous solution, which was double higher than that of the unmodified biochar. The experimental results suggest that the adsorption efficiency of DOX on the Cu-BC is dominated by the strong complexation, electrostatic interactions between DOX molecules and the Cu-BC samples. Comprehensively considering the cost, efficiency and the application to realistic water, the Cu-BC hold the significant potential for enhancing the effectiveness to remove DOX from water.

© 2017 Elsevier B.V. All rights reserved.

**Abbreviations:** DOX, doxycycline hydrochloride; BC, biochar; Cu-BC, copper nitrate modified biochar; SEM, scanning electron microscopy; XRD, X-ray diffraction; XPS, X-ray Photoelectron Spectrometer; FTIR, Fourier transform infrared spectrophotometer.

\* Corresponding authors at: College of Environmental Science and Engineering, Hunan University, Changsha 410082, PR China.

E-mail addresses: [whxu@hnu.edu.cn](mailto:whxu@hnu.edu.cn) (W. Xu), [liuyunguo@hnu.edu.cn](mailto:liuyunguo@hnu.edu.cn) (Y. Liu).

## 1. Introduction

Modern society is confronted with a challenge of antibiotics contaminants, which is harmful to the human health and environment (Kummerer, 2009). Antibiotics are widely applied to improve the human health, prevent and treat infections of plants and animals, as

well as promote the animal husbandry growth (Martinez, 2009). However, some studies indicated that about 30–90% of antibiotics were weakly absorbed and released into the environment as the parent compound (Gao et al., 2012; Liu et al., 2011). The related research pointed out that the antibiotics had been detected potable in surface water and ground water (Ternes, 1998). However, antibiotics in traditional wastewater sewage treatment plants are removed with low efficiency which resulted in higher antibiotic resistance (Ling et al., 2013). DOX, an effective broad-spectrum antibiotic, it is used to treat a number of different bacterial infections which could keep bacteria from reproducing and synthesizing protein (Phaechamud and Charoenteeraboon, 2008; Vargas-Estrada et al., 2008). Their complicated structures and variable physicochemical properties caused their complex behavior in the environment. Developing an efficient, sustainable and economically feasible adsorbent is an effective way to remove the antibiotics pollutants from waste water. Some studies have shown that graphene (Gao et al., 2012), mesoporous silica (Zhang et al., 2015), montmorillonite (Zhao et al., 2012) and carbon nanotubes (Kim et al., 2014; Tang et al., 2014; Zhang et al., 2016) were effective and widely used as sorbent for removing contaminant. However their high cost and complicated process limited their application. BC and activated carbon are the preferred adsorbent for the removal of contaminant from water. They have some favorable physical/chemical surface characteristics such as extensive surface area and well-developed pore structure (Ahmed et al., 2015; Li et al., 2013b; Sun et al., 2013). The raw materials for activated carbon production are mostly obtained from coal and timber which are nonrenewable and relatively expensive. Nevertheless, BC is the pyrolytic product of various waste biomass sources (i.e. forest energy, crop straw, livestock manure, living garbage), which is more environmentally and economically viable (Tan et al., 2015; Wang et al., 2013; Yao et al., 2011). Therefore, BC is a feasible substitute for activated carbon that is widely employed in removing contaminants from aqueous solution. Numerous studies have shown that metallic catalysts modified biochar can enhance the capacity and selectivity for pollutant removal. Wang et al. (Wang et al., 2016) synthesized Ni and Mn oxides biochar and the results showed that the adsorption capacity of the modified BC was increased compared with the pristine biochar. Hu et al. (Hu et al., 2015) studied iron-impregnated biochar and the results indicated that the specific surface areas of the biochar was decreased through iron impregnation, which caused much better sorption of As. Fang et al. (Fang et al., 2014) used Mg modified corn biochar to remove P, and obtained the predictive effect.

In this work, biochar was derived from peanut shell in a N<sub>2</sub> atmosphere at 450 °C without oxidation and then impregnated with Cu(II). Cu(II) has a significant tendency to form complexes in solution with various functional groups present in organic matter, i.e. —COOH and —OH. Selecting DOX as a target pollutant, we investigated the sorption performance of Cu-BC by batch of experiments. The main goals of this work were to: (1) synthesize and characterize the Cu-BC, (2) test the effects of the solution pH and ionic strength on DOX adsorption, adsorption kinetics, adsorption isotherms and the DOX removal ability of the Cu-BC, (3) analyze the sorption mechanism of DOX onto the Cu-BC under different physical and chemical conditions.

## 2. Materials and methods

### 2.1. Materials

Doxycycline hydrochloride (DOX, MW = 480.90, chemical formula C<sub>22</sub>H<sub>24</sub>N<sub>2</sub>O·HCl) was purchased from Rubio Corporation, Germany. The other chemicals including Cu(NO<sub>3</sub>)<sub>2</sub>·2H<sub>2</sub>O, NaOH, HCl, NaCl, KCl, CaCl<sub>2</sub>, MnCl<sub>2</sub>, MgCl<sub>2</sub> were purchased from Municipality Kemi'ou Chemical Reagent Co., Ltd., Tianjin. The biomass peanut shell was collected from Hunan, China. High purified water (18.25 MΩ/cm) from a Millipore MilliQ water purification system was used in all the

experiments. All chemicals employed in the experiments were purchased at analytic purity and used.

### 2.2. Preparation of sorbents

Peanut shells were first washed with high purified water, dried and shattered to pieces. BC was obtained by pyrolyzing the feedstock in a lab-scale tubular reactor (SK-G08123K, China) at 450 °C in a flow of N<sub>2</sub> for 2 h. The BC were modified as follows: 1 g prepared BC and 2 g Cu(NO<sub>3</sub>)<sub>2</sub>·2H<sub>2</sub>O was mixed with 100 mL high purified water in a 200 mL conical flask and then it was shaken in a temperature controlled shaker (SHZ-88, Shanghai) at 150 rpm at 25 °C for 16 h. Then the modified BC was filtered and washed with purified water by vacuum filtration until the pH close to neutral. Finally the sorbent was reserved in desiccators before used.

### 2.3. Characterization methods

The morphology of adsorbent was characterized which was used to compare the structure and surface characteristics of the materials by a field-emission scanning electron microscopy (JEOL JSM-6700, Japan). The X-ray diffraction (XRD) patterns of samples were obtained using an X-ray diffractometer (Rigaku D/max-2500, Japan), with Cu Kα radiation (λ = 1.541 Å) over the 2θ range of 10–80°. The elemental composition of the samples was examined using an ESCALAB 250Xi X-ray Photoelectron Spectrometer (XPS) (Thermo Fisher, USA). Surface organic functional groups of BC were analyzed by a Fourier transform infrared spectrophotometer (FTIR) (Nicolet, 6700 spectrometer, USA). Spectra were obtained at the 4000–400 cm<sup>-1</sup> region. The surface charge of the samples was determined by measuring the zeta potential using an electroacoustic spectrometer (Zetasizer Nano-ZS90, Malvern) under a solution pH varying from 2.0 to 11.0.

### 2.4. Adsorption batch experiment

To avoid photodegradation, all sample flasks or tubes were wrapped by aluminum-foil in all the batch experiments. A stock solution (1000 mg/L) of DOX was always freshly prepared by dissolving 0.2 g of DOX into 1000 mL distilled water during all the experiments. Different DOX concentrations used in batch experiments were obtained through diluting the stock solution. 20 mg/L was the initial concentration of DOX solution. The batch experiments for sorption of DOX were carried out in 100 mL conical flasks containing 0.10 g of Cu-BC and 50 mL DOX solution, then shaken with a speed of 150 rpm for 24 h at 25 °C. The DOX solution pH was adjusted by adding negligible volumes of 0.1 M NaOH or HCl. At predetermined time, the mixture was drawn and separated by filtration. The remaining concentration of DOX in the supernatant was determined on a UV–vis spectrophotometer (UV-2550, SHIMADZU, Japan) at wavelength (k<sub>max</sub>) of 351 nm (Alkhraisat et al., 2010) using calibration curve. Adsorption efficiency *E* (%) and the adsorption capacity *q<sub>e</sub>* (mmol/kg) of DOX were calculated using the following equations:

$$E = \frac{(C_0 - C_e) \times 100\%}{C_0} \quad (1)$$

$$q_e = \frac{(C_0 - C_e)V}{m} \quad (2)$$

where *C*<sub>0</sub> and *C*<sub>e</sub> represent the initial and final concentrations (mmol/L) of DOX in the aqueous phase, respectively. *V* (L) stands for the volume of solution, and *m* (kg) is the mass of sorbent.

### 3. Results and discussion

#### 3.1. Characterization

SEM micrograph of the BC and Cu-BC are shown in Fig. 1. As can be seen in Fig. 1a, BC was basically smooth. The image of Cu-BC (Fig. 1b) revealed that the surface became rough and added some small bits. These might be because Cu had covered or embedded in BC and changed the surface fabrication. Moreover, the rough surface of Cu-BC increased the surface area, which was beneficial for adsorption of the contaminants.

The XRD profiles of the Cu-BC and BC are shown in Fig. 2. The first strong and sharp peak was observed at  $2\theta = 15.6^\circ$  of Cu-BC, which was consistent with the standard XRD data for the orthorhombic phase  $\text{Cu}(\text{OH})_2$  (Yang et al., 2012). There must be parts of Cu(II) atoms interacted with functional groups (i.e. hydroxyl, and carboxylate) on the surface of BC. Another typical sharp peak at  $2\theta = 26.6^\circ$  was corresponding to the diffraction of C (002) in Cu-BC and BC (Zeng et al., 2014), suggesting that Cu-BC and BC were consisted of aromatic carbon sheets. And compared to BC, some new peaks of Cu-BC appeared at  $31.11^\circ$ ,  $32.45^\circ$ ,  $33.67^\circ$ ,  $34.8^\circ$ ,  $37.45^\circ$ , which could be attributed to introducing a small quantity of oxygen-containing functional groups. The further evidences about the functional groups were provided by the following FT-IR analysis.

The spectra of Cu-BC of C1s, N1s, O1s and Cu2p are shown in Fig. 3. For the C1s XPS spectrum, three peaks at 284.26, 284.64 and 285.46 eV, were attributed to C—C, C—H, C—O (Singh et al., 2014; Yang and Jiang, 2014; Zeng et al., 2016). The three peaks components at approximately 398.29, 400.24, and 401.04 eV were consistent with the nitrogen atoms in the —CONH—, —NH<sub>2</sub> and N—C species (Huang et al., 2016; Peng et al., 2015; Yang et al., 2015), respectively. The O1s spectra could be divided into three peaks at 531.84 eV (C=O), 533.34 eV (C—O—H/C—O—C) (Peng et al., 2015; Xu and Jiang, 2015). These results correspond to the XRD analysis of oxygen-containing

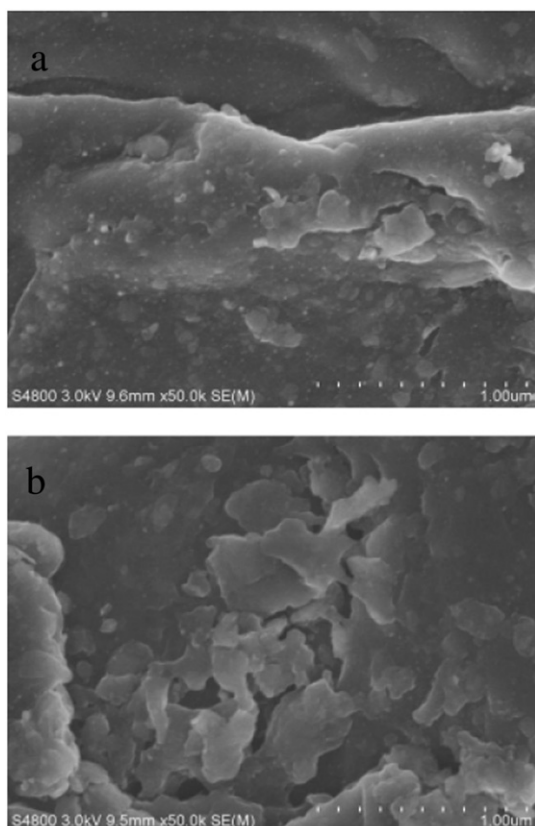


Fig. 1. SEM image of (a) BC, (b) Cu-BC.

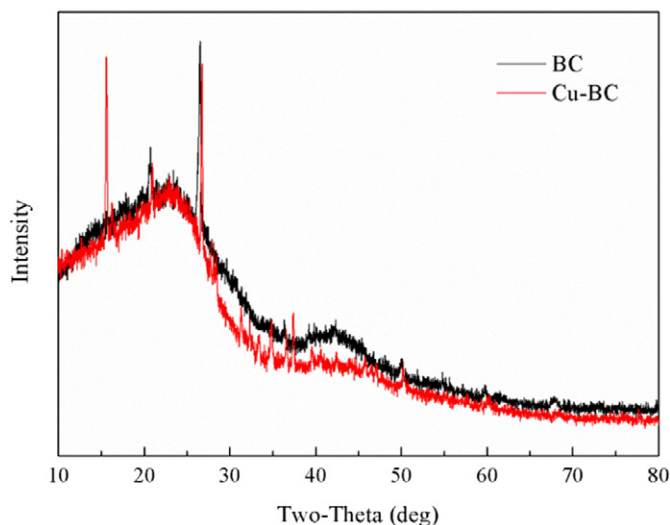


Fig. 2. XRD patterns of BC and Cu-BC.

functional groups. Cu peaks at approximately 934.79 eV, 943.84 eV were shakeup satellite of  $\text{Cu}2p_{1/2}$  and  $\text{Cu}2p_{3/2}$  (Bogusz et al., 2015; Vomacka et al., 2016; Yang et al., 2015), indicating the presence of Cu(II) states. The XPS analysis indicated that the surface of Cu-BC had numerous polar functional groups, which implied that the adsorbent was extremely hydrophilic.

Fig. 4 illustrates the FTIR spectra of the BC and Cu-BC. For BC (Fig. 4(a)), the peak at  $3600\text{ cm}^{-1}$  was fitted to —NH<sub>2</sub> stretching (Prakash et al., 2013). The broad and prominent peak at  $3435\text{ cm}^{-1}$  was typical of the existence of —OH group (Xu et al., 2011). Two peaks at  $1620\text{ cm}^{-1}$  and  $1385\text{ cm}^{-1}$  was described as C=O and —COOH group (Jia et al., 2013; Xu et al., 2013). The band at around  $1060\text{ cm}^{-1}$  could be primarily attributed to the C—O stretch of the alcoholic groups (Dong et al., 2011). Peak around  $1240\text{ cm}^{-1}$  was assigned to phenolic-OH, and the C—H and C—O bending deformation appeared at about  $876, 478\text{ cm}^{-1}$ , respectively (Cao and Harris, 2010; Jia et al., 2013; Zeng et al., 2016). After Cu(II) modification, some significant changes of the function groups were visible (Fig. 4(b)). The —NH<sub>2</sub> stretching band at  $3600\text{ cm}^{-1}$  was shifted to  $3660\text{ cm}^{-1}$ , suggesting the chemical interactions had occurred between the Cu(II) and the —NH<sub>2</sub> groups on BC surface and thus formed Cu—N bond (Prakash et al., 2013). The peak of —OH at  $3435\text{ cm}^{-1}$  and phenolic —OH at  $1240\text{ cm}^{-1}$  migrated to  $3430\text{ cm}^{-1}$  and  $1230\text{ cm}^{-1}$ , respectively, it could be clearly concluded that the Cu(II) could produce a chelation effect with —OH group. The peaks at  $1640$  and  $1385\text{ cm}^{-1}$ , corresponding to the C=O and —COOH group, these peak were shifted to  $1624$  and  $1382\text{ cm}^{-1}$ . Such shift indicated that carbonyl and carboxyl groups might affect the complexation of Cu(II) and BC. Moreover, it was noteworthy that the broad band of  $1050\text{ cm}^{-1}$  shifted to  $1070\text{ cm}^{-1}$ , signifying that the surface chemical state of C—O groups changed after modification. And the peak at wavenumbers  $478\text{ cm}^{-1}$  changed to  $469\text{ cm}^{-1}$ , indicating the formation of Cu—O bond (Siddiqui et al., 2016). These results indicated that the surface functional groups of BC samples were modified by Cu(II) successfully.

#### 3.2. Comparison of adsorption efficiency by modified biochar and pristine biochar

The comparison of adsorption efficiency by Cu-BC and BC was carried out at diverse DOX concentrations (10–100 mg/L) at temperature of  $25^\circ\text{C}$ . As seen in Fig. 5, the DOX adsorption efficiency of the Cu-BC was ranged from 58.07% to 90.56%, it was double higher than the DOX adsorption efficiency of the pristine biochar, which was ranged from 20.49% to 43.38%. And the best adsorption efficiency was 90.56% at

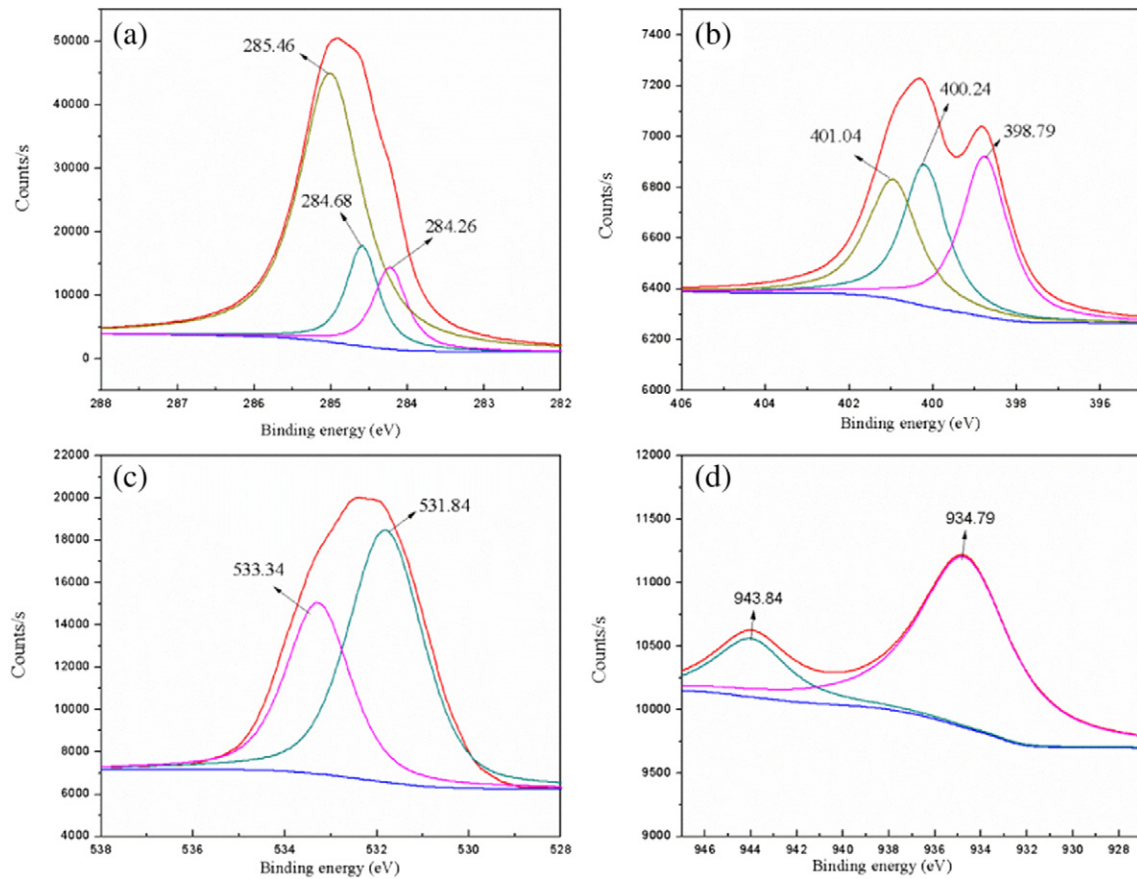


Fig. 3. XPS spectra of (a) C1s, (b) N1s, (c) O1s and (d) Cu2p of Cu-BC.

initial concentration of 20 mg/L. In short, Cu-BC exhibited excellent sorption efficiency compared with pristine biochar.

3.3. Effect of pH on the DOX adsorption

The solution pH is an important factor to investigate the adsorption process, because it can affect the sorption characteristics and the degree of ionization and speciation of the sorbent (Kołodziejńska et al., 2012). The experiment investigated the effect of pH ranged from 2.0–11.0 on sorption. Zeta potential of two samples and DOX sorption efficiency under different pH are measured and illustrated in Fig. 6. The tested materials showed amphoteric properties: The properties of Cu-BC and DOX

might come from both cationic (amine) and anionic (hydroxyl or carboxyl) groups in their molecules. According to the zeta potential-pH profiles, the sorption efficiency of DOX increased quickly at pH < 4.0, slowly at pH 4.0–8.0, and decreased rapidly at pH > 8.0. These phenomena might be attributed to the strong electrostatic interactions between DOX molecules and Cu-BC adsorbent surfaces. The maximum adsorption efficiency (93.22%) was occurred at pH 8.0, because of the difference between positive and negative surface charges reached the largest value of charge. Thus, pH = 8.0 was the optimal pH for the adsorption experiments. And the electrostatic interaction might be a major factor controlling the adsorption process.

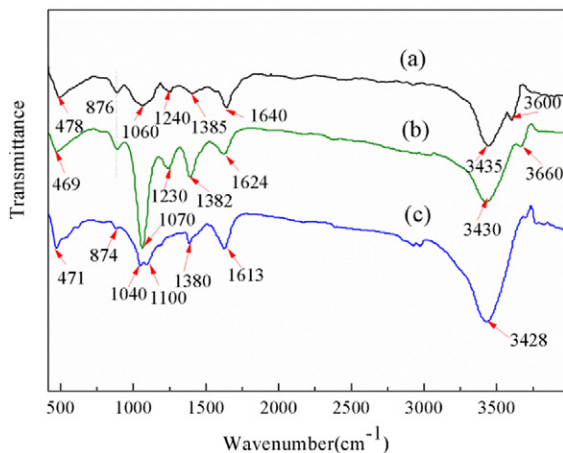


Fig. 4. FTIR spectra of (a) BC, (b) Cu-BC and (c) Cu-BC after DOX adsorption.

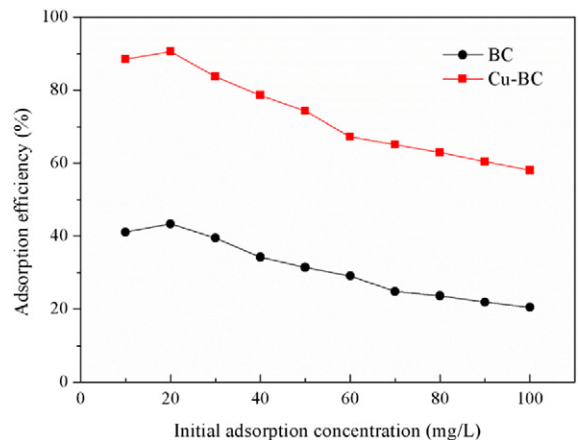


Fig. 5. The comparison of adsorption efficiency on BC and Cu-BC under 298 K.

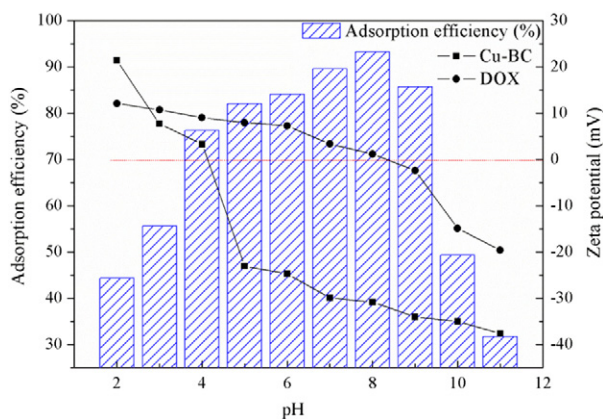


Fig. 6. Effect of the solution pH on adsorption efficiency of DOX by Cu-BC and zeta potentials of DOX, Cu-BC at different pH:  $C_{0(\text{DOX})} = 20 \text{ mg/L}$ ,  $t = 24 \text{ h}$ ,  $T = 298 \text{ K}$ .

### 3.4. Sorption kinetics of DOX

The kinetics of adsorption of DOX is plotted in Fig. 7(a), which determined the rate of DOX removal from wastewater (Li et al., 2013a). At the concentration of 20 mg/L and pH = 8.0, the kinetics experiment

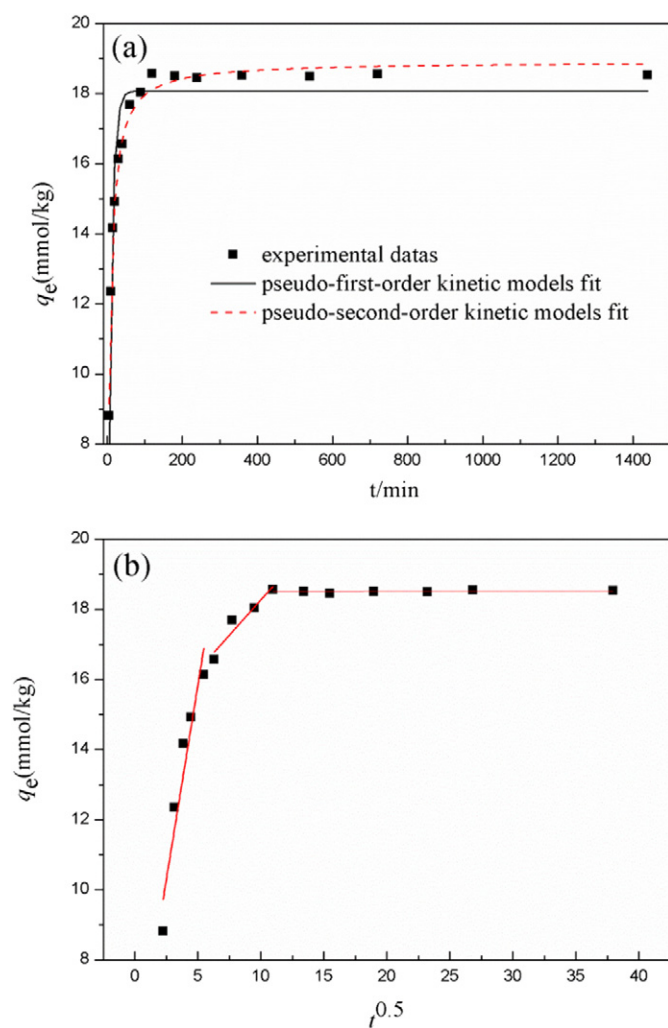


Fig. 7. Kinetics of DOX sorption onto Cu-BC: (a) pseudo-first-order and pseudo-second-order sorption kinetics; (b) intra-particle diffusion kinetics ( $C_{0(\text{DOX})} = 20 \text{ mg/L}$ , pH =  $8.0 \pm 0.2$ ,  $t = 24 \text{ h}$ ,  $T = 298 \text{ K}$ ).

was performed as the contact time from 0 to 24 h in order to determine equilibrium time. As shown in Fig. 7(a), the adsorption of DOX increased quickly in the initial 3 h and then remained relatively stable after 3 h. It demonstrated that the adsorption equilibrium was achieved approximately within 3 h. The nonlinearized equations of pseudo-first-order and pseudo-second-order model were used for the experiment data.

$$\text{pseudo-first-order: } \ln(q_e - q_t) = \ln q_e - k_1 t \quad (3)$$

$$\text{pseudo-second-order: } \frac{t}{q_t} = \frac{1}{k_2 q_e^2} + \frac{t}{q_e} \quad (4)$$

where  $q_e$  and  $q_t$  are the adsorbed concentration (mmol/kg) of DOX at equilibrium and at different time, respectively.  $k_1$  (1/min) and  $k_2$  (kg/mmol min) denote the adsorption rate constants of pseudo-first-order and pseudo-second-order, respectively.

The kinetic parameters calculated from the pseudo-first-order and pseudo-second-order models are listed in Table 1. From Table 1, the determination coefficients of pseudo-second-order model ( $R^2 = 0.993$ ) was higher than the pseudo-first-order model ( $R^2 = 0.929$ ). Besides, comparing the  $q_e$ , pseudo-second-order model fitted with the experimental data much better than those of the pseudo-first-order model. Based on these data analysis, it could be deduced that pseudo-second-order model were obviously better suited for interpreting the adsorption process of DOX, which indicated that the rate-limiting step may be controlled by chemisorption (Tsai and Chen, 2013).

Furthermore, the intra-particle diffusion model was used to furtherly investigate the mechanisms and rate controlling steps of DOX sorption on Cu-BC. The model can be described as (Liu et al., 2011):

$$q_e = k_p t^{0.5} + C \quad (5)$$

where  $k_p$  (mmol/kg min<sup>1/2</sup>) is the constant of intra-particle diffusion rate,  $C$  (mmol/kg) is proportional to the thickness of boundary layer. Fig. 7(b) shows that the sorption process of DOX onto Cu-BC was divided into three stages. The first sharper slope indicated a fast sorption of DOX on the available external surface of Cu-BC. The second portion was due to intra-particle diffusion. At the last equilibrium stage, intra-particle diffusion started to slow down due to the extremely low DOX concentrations, smaller pores and less sorption site (Hameed et al., 2008). And the curve of three stages were not through the origin, which indicated intraparticle diffusion was not the only rate-controlling step in the sorption process (Azza Khaled et al., 2009).

### 3.5. Adsorption isotherm

Equilibrium isotherms have been widely applied to describe the relationship between the adsorbed concentration and equilibrium concentration in the reaction system (Ahmed et al., 2015; Tang et al., 2012). In order to investigate the adsorption behavior in the isotherm reaction system, batch experiments were carried out with different initial concentrations (10–100 mg/L) at pH 8.0. The effect of surfactant sorption isotherms of DOX on Cu-BC are presented in Fig. 8. The experimental data simulated by the commonly isotherm models of Langmuir, Freundlich and Temkin isotherm. The Langmuir model is based on the supposition that monolayer surface adsorption occurs at a monolayer

Table 1  
Pseudo-first-order and pseudo-second-order kinetic models of DOX adsorption on the Cu-BC.

$q_{e,\text{exp}}$	Pseudo-first-order			Pseudo-second-order		
	$q_{e,1}$ (mmol/kg)	$K_1$ (1/min)	$R^2$	$q_{e,2}$ (mmol/kg)	$K_2$ (kg/mmol min)	$R^2$
18.764	18.073	0.107	0.929	18.916	0.001	0.993

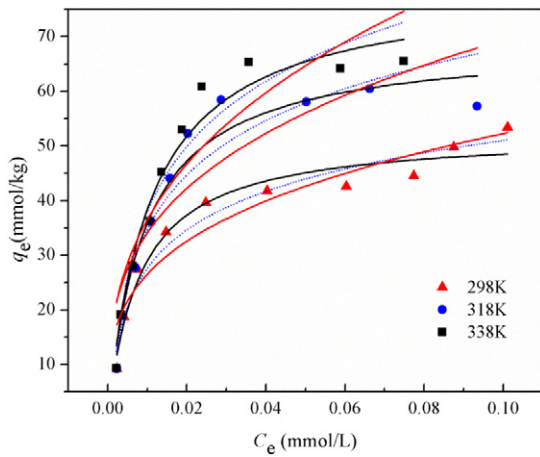


**Fig. 8.** DOX sorption isotherms with Cu-BC at three different temperatures:  $C_{0(\text{DOX})} = 10\text{--}100$  mg/L, pH =  $8.0 \pm 0.2$ ,  $t = 3$  h. The black and red solid lines are the Langmuir and Freundlich model simulation; the dashed lines are the Temkin model simulation.

and equivalent sorption energies system without any interaction between the adsorbed pollutants (Guo et al., 2015).

The Langmuir equation is expressed in the following equation:

$$q_e = \frac{K_L q_m C_e}{1 + K_L C_e} \quad (6)$$

where  $q_e$  (mmol/kg) is the equilibrium adsorption concentration and  $q_m$  (mmol/kg) stand for the maximum adsorption capacity of the adsorbent.  $C_e$  (mmol/L) is the equilibrium solution phase concentration, while  $K_L$  (L/kg) is the Langmuir constant.

Freundlich is an empirical equation employed to describe the adsorption process on a heterogeneous surface (Zeng et al., 2016). The Freundlich equation is an empirical equation and presented as here (Eq. (7)).

$$q_e = K_f C_e^n \quad (7)$$

where  $q_e$  (mmol/kg) is the adsorbed value of adsorbate at equilibrium,  $C_e$  (mmol/L) is the equilibrium solute concentration,  $K_f$  ((mmol/kg)(L/mmol)<sup>n</sup>) is the constant indicative of the relative adsorption capacity of the adsorbent and  $n$  (dimensionless) is the exponential parameter.

Temkin model assumes that the heat of sorption of all molecules in the layer would decrease linearly, because of the interaction between adsorbent and adsorbate (Ghorbani-Khosrowshahi and Behnajady, 2016). This model is given as (Ozacar and Sengil, 2005):

$$q_e = B \ln A_T + B \ln C_e \quad (8)$$

where  $R$  (8.314 J/mol/K) is universal gas constant,  $T$  (K) is absolute temperature,  $A_T$  is Temkin isotherm equilibrium binding constant (L/kg),  $B$  (J/mmol) is constant related to heat of adsorption.

Fig. 8 shows the Langmuir, Freundlich and Temkin non-linear fitting curves for DOX adsorption and the constants are listed in Table 2.

**Table 2**  
Langmuir and Freundlich isotherm kinetic models of DOX adsorption on the Cu-BC.

T(k)	Langmuir model			Freundlich model			Temkin model		
	$q_m$	$K_L$	$R^2$	$K_f$	$n$	$R^2$	$A_T$	$B$	$R^2$
298	52.374	0.124	0.959	103.014	0.295	0.906	1.513	10.160	0.958
318	69.065	0.108	0.956	141.203	0.309	0.792	1.117	14.383	0.907
338	93.498	0.079	0.965	183.728	0.356	0.838	0.214	17.230	0.940

Clearly, increasing temperature was conducive to enhance adsorption. In addition, it was found Langmuir Adsorption model had the highest correlation coefficients ( $R^2$ ) values at different temperatures and hence the best fit, compared with others model. This result suggested that the adsorbent surface formed monolayer without any interaction between the adsorbent and substrate. Calculated from the Langmuir equation, it could be seen that the maximum adsorption capacity ( $q_e$ ) occurred at 338 K. The values of  $K_L$  were found to be much lower than 1.0, which was beneficial for DOX sorption under three temperatures (Qin et al., 2016). Moreover, this consequence could be proved by all the  $n$  values from Table 2, because when the  $n$  is equal to 1, the sorption was linear, for the values < 1, the sorption process was chemical, and if it was > 1, the sorption would be a physical process. The most surface heterogeneity occurred when the value of  $n$  was near to zero (Ghorbani-Khosrowshahi and Behnajady, 2016). And all the  $n$  values were lower than 0.4 and higher than 0.2, which was better conformed the previous conclusion. These data denoted the strong interaction between the Cu-BC and DOX. Therefore, Cu-BC was an outstanding adsorbent for DOX removal.

### 3.6. Adsorption thermodynamic studies

The equilibrium sorption amounts of DOX were examined to get thermodynamic parameters, with the initial concentrations of 20 mg/L at 298, 308 and 318 K. The effect of temperatures on the adsorption of DOX molecules by adsorbent could be calculated by the following equations.

$$\Delta G^\circ = -RT \ln K^\circ \quad (9)$$

$$\ln K^\circ = -\frac{\Delta H^\circ}{RT} + \frac{\Delta S^\circ}{R} \quad (10)$$

where  $R$  (8.314 J/mol K) is the universal gas constant,  $\Delta G^\circ$  Gibb is free energy,  $\Delta H^\circ$  (KJ/mol) is the total enthalpy of the solution,  $\Delta S^\circ$  (J/mol K) was the entropy of the reaction in solution.  $K^\circ$  was the thermodynamic equilibrium constant, representing the adsorption capacity of the adsorbent to retain the adsorbate and extent of movement of the adsorbate within the solution.  $K^\circ$  could be calculated by plotting  $\ln K_d$  ( $K_d = q_e / C_e$ ) versus  $C_e$  and extrapolating  $C_e$  to zero. The  $\Delta H^\circ$  and  $\Delta S^\circ$  values were calculated from the slope and intercept by plotting  $\ln K^\circ$  against  $1/T$ . The calculated parameters were shown in Table 3.

The sorption process was a spontaneous action because all the  $\Delta G^\circ$  values were negative. With the increase of temperature, the values of  $\Delta G^\circ$  decreased slightly, which revealed the improvement of the adsorption by increasing the temperature. The positive  $\Delta H^\circ$  value indicated the endothermic nature of adsorption, which fitted well with the result that the sorption of DOX increased along with the increase of temperature (Fig. 8). In addition, the positive  $\Delta S^\circ$  indicated that the degrees of freedom increased at the liquid interface during the sorption process.

### 3.7. Effect of background electrolyte

Existing cations may affect adsorption equilibrium of aqueous phase. Therefore, studying adsorption influence of main cations ( $\text{Na}^+$ ,  $\text{K}^+$ ,  $\text{Ca}^{2+}$ ,  $\text{Mg}^{2+}$ ,  $\text{Mn}^{2+}$ ) on DOX was important. It was investigated by adding 0.01 to 1.0 mg/L concentrations of coexisting cations into the reaction system with initial DOX concentration at 298 K and pH 8.0. Fig 9

**Table 3**  
Thermodynamic analysis data for DOX adsorption onto Cu-BC.

T(K)	$\ln K^\circ$	$\Delta G^\circ$ (kJ/mol)	$\Delta S^\circ$ (J/k mol)	$\Delta H^\circ$ (kJ/mol)
298	8.190	-2.029	68.136	13.957
308	8.373	-2.144		
318	8.461	-2.237		

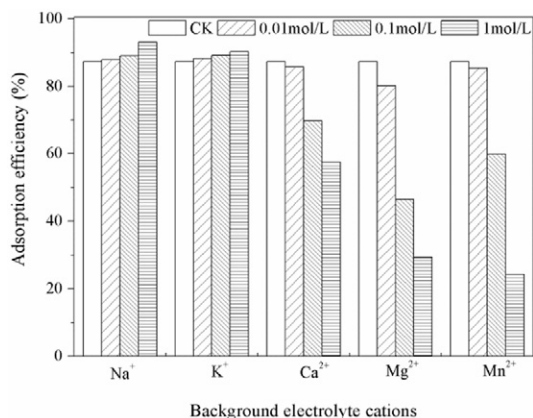


**Fig. 9.** Effects of background electrolyte cations on the adsorption efficiency of DOX by Cu-BC:  $C_{0(\text{DOX})} = 20 \text{ mg/L}$ ,  $\text{pH} = 8.0 \pm 0.2$ ,  $t = 3 \text{ h}$ ,  $T = 298 \text{ K}$ .

showed that the equilibrium sorption efficiency was influenced by the existence of cations.  $\text{Na}^+$ ,  $\text{K}^+$  promoted the adsorption of DOX while the  $\text{Ca}^{2+}$ ,  $\text{Mg}^{2+}$ ,  $\text{Mn}^{2+}$  inhibited. The effect of promotion/inhibition enhanced with the increase of concentration. Obviously, the effect of the divalent cations were higher than monovalent cations, and the adsorption efficiency of  $\text{Na}^+$ ,  $\text{K}^+$  was little difference, which suggested that DOX adsorption onto Cu-BC was little sensitive to the with the same ionic strength, but it was very sensitive to the ionic strength. These phenomena could be explained as follows. On the one hand, salting-out effect was always greater than the squeezing-out effect due to divalent cations had higher polarizing power and ionic strength than monovalent cations (Jiang et al., 2016). On the other hand, the relative sorption at higher ionic strength was tremendously affected, which might suggest that special interactions and the formation of DOX complexation were existed except electrostatic sorption. Furthermore, the higher covalent property of divalent cations than monovalent cations could cause stronger direct hydration and reduce its interaction with active sites on the surface of Cu-BC. Therefore, the cations had an important effect on uptake of DOX.

### 3.8. Mechanisms of DOX adsorption on Cu-BC

In order to investigate the interaction mechanism between adsorbate and adsorbent, the FTIR spectra for Cu-BC before and after adsorption with DOX were measured and presented in Fig. 4. The spectra of adsorption onto Cu-BC are shown in Fig. 4(c). Compared to Cu-BC Fig. 4(b), it could be observed that the band at 3430, 1624, 1382, 876, 469  $\text{cm}^{-1}$  was slightly lower than that before sorption, indicating that possible interactions occurred between DOX species with Cu(II) or other functional groups on the sorbent. The Cu—N bending band at 3660  $\text{cm}^{-1}$  became undetectable after reacted with DOX, suggesting more strong groups in DOX competed with N atoms to chelate with Cu(II). The band at 1070  $\text{cm}^{-1}$  were split and shifted to 1040 and 1100  $\text{cm}^{-1}$ . The new peak at 1100  $\text{cm}^{-1}$  was Cu—OH in Cu(II) hydroxide species (Yang et al., 2015), which implied a complexation effect between Cu(II) and —OH on DOX species. Correspondingly, the band at 1230  $\text{cm}^{-1}$  was disappeared, verifying the complexation effect between Cu(II) and DOX species. Taking all the observations and analysis above into account, the presence of  $-\text{NH}_2$  and large amounts of active oxygen-containing functional groups (C—O, C=O, —OH and  $-\text{COO}^-$ ) on BC could react with Cu(II) to form surface complexes, and thus formed Cu-DOX complexes (Jia et al., 2013; Zhao et al., 2012). These may be responsible for DOX adsorption. Therefore, complexation is a significant sorption mechanism of between DOX and Cu-BC.

According to the results of pH-zeta potential measurement and above-mentioned discussion of mechanism, it could be concluded that

DOX was adsorbed by the Cu-BC through the electrostatic interaction and complexation.

## 4. Conclusions

In summary, the fabricated Cu-BC as high-performance adsorbents possessed promising potentials for removing DOX. The DOX removal by Cu-BC was greatly pH dependent and the optimal pH was 8.0. The kinetics and isotherm data could be well described by pseudo-second-order kinetic model and Langmuir model. Thermodynamic results indicated the sorption process was spontaneous and endothermic. The coexisting cation had different influence on DOX adsorption to Cu-BC: the adsorption of DOX slightly facilitated by  $\text{Na}^+$ ,  $\text{K}^+$  and inhibited by  $\text{Ca}^{2+}$ ,  $\text{Mg}^{2+}$ ,  $\text{Mn}^{2+}$ . Main sorption mechanisms of DOX to Cu-BC were electrostatic interaction and surface complexation. Therefore, Cu-BC would provide a cost-effective, realistic efficient and potential sorbent for removing DOX and other persistent organic pollutants from water in the further study.

## Acknowledgments

This research was financially supported by the National Natural Science Foundation of China (Grant Nos. 51609268, 51108167 and 51521006), and the Hunan Provincial Innovation Foundation for Postgraduate (Grant Nos. CX2015B090 and CX2016B135).

## References

- Ahmed, M.B., Zhou, J.L., Ngo, H.H., Guo, W., 2015. Adsorptive removal of antibiotics from water and wastewater: progress and challenges. *Sci. Total Environ.* 532, 112–126.
- Alkhrasat, M.H., Rueda, C., Cabrejos-Azama, J., Lucas-Aparicio, J., Marino, F.T., Torres Garcia-Denche, J., Jerez, L.B., Gbureck, U., Cabarcos, E.L., 2010. Loading and release of doxycycline hyclate from strontium-substituted calcium phosphate cement. *Acta Biomater.* 6 (4), 1522–1528.
- Azza Khaled, A.E.N., El-Sikaily, Amany, Abdelwahab, Ola, 2009. Treatment of artificial textile dye effluent containing direct yellow 12 by orange peel carbon. *Desalination* 238, 210–232.
- Bogusz, A., Oleszczuk, P., Dobrowolski, R., 2015. Application of laboratory prepared and commercially available biochars to adsorption of cadmium, copper and zinc ions from water. *Bioresour. Technol.* 196, 540–549.
- Cao, X., Harris, W., 2010. Properties of dairy-manure-derived biochar pertinent to its potential use in remediation. *Bioresour. Technol.* 101 (14), 5222–5228.
- Dong, X., Ma, L.Q., Li, Y., 2011. Characteristics and mechanisms of hexavalent chromium removal by biochar from sugar beet tailing. *J. Hazard. Mater.* 190 (1–3), 909–915.
- Fang, C., Zhang, T., Li, P., Jiang, R.F., Wang, Y.C., 2014. Application of magnesium modified corn biochar for phosphorus removal and recovery from swine wastewater. *Int. J. Environ. Res. Public Health* 11 (9), 9217–9237.
- Gao, Y., Li, Y., Zhang, L., Huang, H., Hu, J., Shah, S.M., Su, X., 2012. Adsorption and removal of tetracycline antibiotics from aqueous solution by graphene oxide. *J. Colloid Interface Sci.* 368 (1), 540–546.
- Ghorbani-Khosrowshahi, S., Behnajady, M.A., 2016. Chromium(VI) adsorption from aqueous solution by prepared biochar from Onopordom Heteracanthom. *Int. J. Environ. Sci. Technol.* 13 (7), 1803–1814.
- Guo, F.-Y., Liu, Y.-G., Wang, H., Zeng, G.-M., Hu, X.-J., Zheng, B.-H., Li, T.-T., Tan, X.-F., Wang, S.-F., Zhang, M.-M., 2015. Adsorption behavior of Cr(VI) from aqueous solution onto magnetic graphene oxide functionalized with 1,2-diaminocyclohexanetetraacetic acid. *RSC Adv.* 5 (56), 45384–45392.
- Hameed, B.H., Tan, I.A.W., Ahmad, A.L., 2008. Adsorption isotherm, kinetic modeling and mechanism of 2,4,6-trichlorophenol on coconut husk-based activated carbon. *Chem. Eng. J.* 144 (2), 235–244.
- Hu, X., Ding, Z., Zimmerman, A.R., Wang, S., Gao, B., 2015. Batch and column sorption of arsenic onto iron-impregnated biochar synthesized through hydrolysis. *Water Res.* 68, 206–216.
- Huang, X., Liu, Y., Liu, S., Tan, X., Ding, Y., Zeng, G., Zhou, Y., Zhang, M., Wang, S., Zheng, B., 2016. Effective removal of Cr(VI) using  $\beta$ -cyclodextrin-chitosan modified biochars with adsorption/reduction bifunctional roles. *RSC Adv.* 6 (1), 94–104.
- Jia, M., Wang, F., Bian, Y., Jin, X., Song, Y., Kengara, F.O., Xu, R., Jiang, X., 2013. Effects of pH and metal ions on oxytetracycline sorption to maize-straw-derived biochar. *Bioresour. Technol.* 136, 87–93.
- Jiang, L.-H., Liu, Y.-G., Zeng, G.-M., Xiao, F.-Y., Hu, X.-J., Hu, X., Wang, H., Li, T.-T., Zhou, L., Tan, X.-F., 2016. Removal of 17 $\beta$ -estradiol by few-layered graphene oxide nanosheets from aqueous solutions: external influence and adsorption mechanism. *Chem. Eng. J.* 284, 93–102.
- Kim, H., Hwang, Y.S., Sharma, V.K., 2014. Adsorption of antibiotics and iopromide onto single-walled and multi-walled carbon nanotubes. *Chem. Eng. J.* 255, 23–27.
- Kolodyńska, D., Wnętrzak, R., Leahy, J.J., Hayes, M.H.B., Kwapiński, W., Hubicki, Z., 2012. Kinetic and adsorptive characterization of biochar in metal ions removal. *Chem. Eng. J.* 197, 295–305.

- Kummerer, K., 2009. The presence of pharmaceuticals in the environment due to human use—present knowledge and future challenges. *J. Environ. Manag.* 90 (8), 2354–2366.
- Li, G., Zhang, D., Wang, M., Huang, J., Huang, L., 2013a. Preparation of activated carbons from *Iris tectorum* employing ferric nitrate as dopant for removal of tetracycline from aqueous solutions. *Ecotoxicol. Environ. Saf.* 98, 273–282.
- Li, M., Liu, Q., Guo, L., Zhang, Y., Lou, Z., Wang, Y., Qian, G., 2013b. Cu(II) removal from aqueous solution by *Spartina alterniflora* derived biochar. *Bioresour. Technol.* 141, 83–88.
- Ling, C., Liu, F.Q., Xu, C., Chen, T.P., Li, A.M., 2013. An integrative technique based on synergistic core-removal and sequential recovery of copper and tetracycline with dual-functional chelating resin: roles of amine and carboxyl groups. *ACS Appl. Mater. Interfaces* 5 (22), 11808–11817.
- Liu, H., Liu, W., Zhang, J., Zhang, C., Ren, L., Li, Y., 2011. Removal of cephalexin from aqueous solutions by original and Cu(II)/Fe(III) impregnated activated carbons developed from lotus stalks kinetics and equilibrium studies. *J. Hazard. Mater.* 185 (2–3), 1528–1535.
- Martinez, J.L., 2009. Environmental pollution by antibiotics and by antibiotic resistance determinants. *Environ. Pollut.* 157 (11), 2893–2902.
- Ozacar, M., Sengil, I.A., 2005. Adsorption of metal complex dyes from aqueous solutions by pine sawdust. *Bioresour. Technol.* 96 (7), 791–795.
- Peng, W., Xie, Z., Cheng, G., Shi, L., Zhang, Y., 2015. Amino-functionalized adsorbent prepared by means of Cu(II) imprinted method and its selective removal of copper from aqueous solutions. *J. Hazard. Mater.* 294, 9–16.
- Phaechamud, T., Charoenteeraboon, J., 2008. Antibacterial activity and drug release of chitosan sponge containing doxycycline hyclate. *AAPS PharmSciTech* 9 (3), 829–835.
- Prakash, O., Singh, S.K., Singh, B., Singh, R.K., 2013. Investigation of coordination properties of isolated adenine to copper metal: a systematic spectroscopic and DFT study. *Spectrochim. Acta A Mol. Biomol. Spectrosc.* 112, 410–416.
- Qin, L., Zhou, Z., Dai, J., Ma, P., Zhao, H., He, J., Xie, A., Li, C., Yan, Y., 2016. Novel N-doped hierarchically porous carbons derived from sustainable shrimp shell for high-performance removal of sulfamethazine and chloramphenicol. *J. Taiwan Inst. Chem. Eng.* 62, 228–238.
- Siddiqui, H., Qureshi, M.S., Haque, F.Z., 2016. Effect of copper precursor salts: facile and sustainable synthesis of controlled shaped copper oxide nanoparticles. *Optik* 127 (11), 4726–4730.
- Singh, B., Fang, Y., Cowie, B.C.C., Thomsen, L., 2014. NEXAFS and XPS characterisation of carbon functional groups of fresh and aged biochars. *Org. Geochem.* 77, 1–10.
- Sun, L., Wan, S., Luo, W., 2013. Biochars prepared from anaerobic digestion residue, palm bark, and eucalyptus for adsorption of cationic methylene blue dye: characterization, equilibrium, and kinetic studies. *Bioresour. Technol.* 140, 406–413.
- Tan, X., Liu, Y., Zeng, G., Wang, X., Hu, X., Gu, Y., Yang, Z., 2015. Application of biochar for the removal of pollutants from aqueous solutions. *Chemosphere* 125, 70–85.
- Tang, W.-W., Zeng, G.-M., Gong, J.-L., Liu, Y., Wang, X.-Y., Liu, Y.-Y., Liu, Z.-F., Chen, L., Zhang, X.-R., Tu, D.-Z., 2012. Simultaneous adsorption of atrazine and Cu(II) from wastewater by magnetic multi-walled carbon nanotube. *Chem. Eng. J.* 211–212, 470–478.
- Tang, W.W., Zeng, G.M., Gong, J.L., Liang, J., Xu, P., Zhang, C., Huang, B.B., 2014. Impact of humic/fulvic acid on the removal of heavy metals from aqueous solutions using nanomaterials: a review. *Sci. Total Environ.* 468–469, 1014–1027.
- Termes, T.A., 1998. Occurrence of drugs in German sewage treatment plants and rivers. *Water Res.* 32 (11), 3245–3260.
- Tsai, W.T., Chen, H.R., 2013. Adsorption kinetics of herbicide paraquat in aqueous solution onto a low-cost adsorbent, swine-manure-derived biochar. *Int. J. Environ. Sci. Technol.* 10 (6), 1349–1356.
- Vargas-Estrada, D., Gracia-Mora, J., Sumano, H., 2008. Pharmacokinetic study of an injectable long-acting parenteral formulation of doxycycline hyclate in calves. *Res. Vet. Sci.* 84 (3), 477–482.
- Vomacka, P., Stengl, V., Henych, J., Kormunda, M., 2016. Shape-controlled synthesis of Sn-doped CuO nanoparticles for catalytic degradation of Rhodamine B. *J. Colloid Interface Sci.* 481, 28–38.
- Wang, B., Li, C., Liang, H., 2013. Bioleaching of heavy metal from woody biochar using *Acidithiobacillus ferrooxidans* and activation for adsorption. *Bioresour. Technol.* 146, 803–806.
- Wang, S., Gao, B., Li, Y., 2016. Enhanced arsenic removal by biochar modified with nickel (Ni) and manganese (Mn) oxyhydroxides. *J. Ind. Eng. Chem.* 37, 361–365.
- Xu, H., Jiang, H., 2015. Effects of cyanobacterial extracellular polymeric substances on the stability of ZnO nanoparticles in eutrophic shallow lakes. *Environ. Pollut.* 197, 231–239.
- Xu, R.K., Xiao, S.C., Yuan, J.H., Zhao, A.Z., 2011. Adsorption of methyl violet from aqueous solutions by the biochars derived from crop residues. *Bioresour. Technol.* 102 (22), 10293–10298.
- Xu, X., Cao, X., Zhao, L., 2013. Comparison of rice husk- and dairy manure-derived biochars for simultaneously removing heavy metals from aqueous solutions: role of mineral components in biochars. *Chemosphere* 92 (8), 955–961.
- Yang, G.X., Jiang, H., 2014. Amino modification of biochar for enhanced adsorption of copper ions from synthetic wastewater. *Water Res.* 48, 396–405.
- Yang, Y.J., Li, W., Chen, X., 2012. Highly enhanced electrocatalytic oxidation of glucose on Cu(OH)<sub>2</sub>/CuO nanotube arrays modified copper electrode. *J. Solid State Electrochem.* 16 (9), 2877–2881.
- Yang, Z., Jia, S., Zhang, T., Zhuo, N., Dong, Y., Yang, W., Wang, Y., 2015. How heavy metals impact on flocculation of combined pollution of heavy metals-antibiotics: a comparative study. *Sep. Purif. Technol.* 149, 398–406.
- Yao, Y., Gao, B., Inyang, M., Zimmerman, A.R., Cao, X., Pullammanappallil, P., Yang, L., 2011. Biochar derived from anaerobically digested sugar beet tailings: characterization and phosphate removal potential. *Bioresour. Technol.* 102 (10), 6273–6278.
- Zeng, D., Liu, S., Gong, W., Wang, G., Qiu, J., Chen, H., 2014. Synthesis, characterization and acid catalysis of solid acid from peanut shell. *Appl. Catal. A Gen.* 469, 284–289.
- Zeng, W., Liu, Y.-G., Hu, X.-J., Liu, S.-B., Zeng, G.-M., Zheng, B.-H., Jiang, L.-H., Guo, F.-Y., Ding, Y., Xu, Y., 2016. Decontamination of methylene blue from aqueous solution by magnetic chitosan lignosulfonate grafted with graphene oxide: effects of environmental conditions and surfactant. *RSC Adv.* 6 (23), 19298–19307.
- Zhang, Z., Liu, H., Wu, L., Lan, H., Qu, J., 2015. Preparation of amino-Fe(III) functionalized mesoporous silica for synergistic adsorption of tetracycline and copper. *Chemosphere* 138, 625–632.
- Zhang, C., Lai, C., Zeng, G., Huang, D., Yang, C., Wang, Y., Zhou, Y., Cheng, M., 2016. Efficacy of carbonaceous nanocomposites for sorbing ionizable antibiotic sulfamethazine from aqueous solution. *Water Res.* 95, 103–112.
- Zhao, Y., Gu, X., Gao, S., Geng, J., Wang, X., 2012. Adsorption of tetracycline (TC) onto montmorillonite: cations and humic acid effects. *Geoderma* 183–184, 12–18.